Isopycnal Empirical orthogonal Functions (EOFs) in the North and Tropical Atlantic and their use in estimation problems.

Pascal Faucher, Michel Gavart, Pierre De Mey

Isopycnal empirical orthogonal functions (EOFs) in the North and tropical Atlantic and their use in estimation problems

P. Faucher, M. Gavart, and P. De Mey
Laboratories d'Etudes en Géophysique et Océanographie Spatiales, Toulouse, France

Received 26 October 2000; revised 5 September 2001; accepted 3 October 2001; published 16 August 2002.

[1] We investigated the vertical variability of the thermal/dynamical structure of the North and tropical Atlantic ocean from a set of historical hydrographic data [*Reynaud et al.*, 1998]. The analysis was performed in 10° geographic bins in terms of vertical empirical orthogonal functions (EOFs) in isopycnal coordinates as first proposed by *Gavart and De Mey* [1997] (hereinafter referred to as GDM97). In the isopycnal coordinate system the state vector is made up of isopycnal displacements (η) and the compensated potential temperature along isopycnals (θ). GDM97 showed that in the Azores-Madeira region the isopycnal EOFs consistently help to better separate physical processes in the water column and to better project the dynamic height anomaly downward in comparison with the classical EOF analysis in depth coordinates. In the present study, we extended their work geographically and the connection with state estimation and data assimilation was more formalized. From our results, smooth spatial variations of isopycnal EOFs were found in the North Atlantic and confirmed the large-scale relevance of isopycnal EOFs in the ocean. North of 20°N the dominant isopycnal EOF was associated with a quasihomogeneous vertical displacement of the isopycnal surfaces ($\eta \approx 1$) with a quasiconservation of compensated potential temperature on those surfaces ($\theta \approx 0$). That mode was strongly modified by thermocline-intensified baroclinic effects along the path of the Gulf Stream up to 40°W. Some physical interpretations of the vertical EOFs were also suggested in several areas as far as the isopycnal formulation was concerned (e.g., some thermal fronts, the Mediterranean outflow, water lenses, or "meddies"). This work confirmed the validity of the ideas of GDM97 over the entire North Atlantic ocean. The potential use of the isopycnal EOFs in state estimation problems was discussed. They are possible candidates to reduce the order of state estimation problems provided that they have good observability properties. These observability properties were studied in the case of satellite altimetry; that is, we examined how the dominant isopycnal EOFs were connected to sea-level anomalies. In most bins it was found that the order of an estimation problem could be truncated to one (primarily north of 20°N) or two modes. The dominant EOF was found to account for most of the surface dynamic height variability with a rather normally distributed error of only a few centimeters. Dynamically more robust results were also presented, performing a univariate isopycnal analysis in η, leaving coherent thermal effects out. As a result, the dominant character of mode 1 was further enhanced everywhere. These univariate isopycnal EOFs can be used for purely dynamical state estimation. More generally, we believe that our results can be used to set up reduced-order data assimilation schemes in the North Atlantic or in other regions with good historical data. *INDEX TERMS:* 4536 Oceanography: Physical: Hydrography; 4283 Oceanography: General: Water masses; 4532 Oceanography: Physical: General circulation; 4528 Oceanography: Physical: Fronts and jets; 4263 Oceanography: General: Ocean prediction; *KEYWORDS:* North Atlantic, vertical variability, EOFs, isopycnal coordinates, order reduction, state estimation

1. Introduction

[2] The vertical empirical orthogonal function (EOF) analysis is widely used in dynamical oceanography as a tool to extract the vertically coherent processes with the largest variability [e.g., *Hayes and Halpern*, 1984; *Mercier and Colin de Verdière*, 1985; *Fukumori and Wunsch*, 1991; *Mercier et al.*, 1993; *Wunsch*, 1997; *Maes*, 1999]. Vertical EOFs can be calculated from in situ data such as vertical profiles, currentmeters, etc., or from numerical model out-

0148-0227/02/2000JC000690

puts. The interest for vertical EOFs in the oceanographic community is based on the fact that, although statistical in essence, they give insight into the coherent structure and amplitude of the dominant processes, dynamical and thermodynamical, present in the surface and subsurface layers. Their relative amplitudes in space and time give a measure of the vertical structure of the variability in the ocean.

[3] Vertical EOFs and other statistical methods have also been used to relate the surface dynamic height to subsurface variables since satellite altimetry provides most of the routine global observations of the oceans [e.g., *Carnes et al.*, 1990; *Mellor and Ezer*, 1991; *Fischer and Latif*, 1995]. For instance, *Carnes et al.* [1990] reconstructed the thermal structure of a small domain surrounding the Gulf Stream from altimeter-derived sea surface heights using third-order polynomial regression relationships between dynamic height and amplitudes of EOFs of the vertical structure of temperature. The resulting temperature estimates have an rms error of $\sim$1°C below 200 m. The error increases to 2°C near the surface, where there is significant change in temperature caused by the annual cycle of heat exchange with the atmosphere.

[4] Vertical EOFs have also been used extensively in the recent years to give a particular vertical structure to model errors in the framework of ocean data assimilation [e.g., *De Mey and Robinson*, 1987; *Rienecker and Adamec*, 1995; *Gavart et al.*, 1999; *De Mey and Benkiran*, 2002]. It is assumed, in particular, that background and forecast errors can be expressed efficiently on a set of functions derived from empirical data analysis, i.e., that databased EOFs define dominant error directions along which the model trajectory can be corrected efficiently using the incoming data. Since, in general, only a few EOFs are used, this truncation process comes back to a reduction of the order of the error subspace. It is therefore of the highest priority to examine how the new error subspace is connected to the observations, i.e., how the observability problem is modified by the EOF order reduction.

[5] We will calculate the dominant EOFs and discuss their use in estimation problems in the context of the North and tropical Atlantic, for which an extensive hydrographical historical database does exist. An original aspect of the present work is to carry out the calculations in isopycnal coordinates. *Gavart and De Mey* [1997] (hereinafter referred to as GDM97) were among the first to use the isopycnal coordinate system for their EOF calculations in the Azores-Madeira region. Here we extend their work geographically since the whole North Atlantic between the equator and 50°N is covered. The connection with state estimation and data assimilation is also more formalized. Our variables will be the depth of selected isopycnal surfaces and the potential temperature along these surfaces. As in GDM97, by using this set of variables, our initial scope is therefore to study the coherent dynamical and thermodynamical variability of the regions covered by the data set. Statistical tools such as EOFs are able to quantify such correlations (or lack thereof) between variables. In particular, it was shown by GDM97 that in most of the cases studied, the use of isopycnal coordinates helped to better separate the vertical physical processes present in the water column when compared to *z*-coordinate EOFs. There are other reasons for computing statistics in the isopycnal space. We expect isopycnal EOFs to have a larger geographical domain of validity than, for example, *z*-based EOFs since the large-scale properties in the ocean are more naturally followed on isopycnal surfaces [e.g., *Pedlosky*, 1987]. There is also a growing interest in isopycnal circulation models potentially implied in estimation problems [*Bleck and Smith*, 1990; *Chassignet*, 1992; *New and Bleck*, 1995; *Smith et al.*, 2000]. Finally, the reduced-order observability problem for altimetry (one of the most continuous ocean data source nowadays) is more naturally studied in isopycnal coordinates because the displacement part is the largest contribution of deep ocean dynamics to the sea-level changes.

[6] The paper is organized as follows. Section 2 briefly presents the in situ data set and its processing. Section 3 describes the methodology used for the calculation of isopycnal bivariate EOFs in an oceanic basin. In section 4 we describe and discuss the results of the isopycnal EOF calculations in the North and tropical Atlantic. In section 5 the potential use of these EOFs in estimation problems is discussed. Finally, results are summarized and conclusions are presented in section 6.

2. Data Set and Preprocessing

[7] Approximately 90,000 conductivity-temperature-depth (CTD)-based temperature and salinity profiles, originating mostly from the National Oceanographic Data Center archives, are obtained with the additional assistance of several international World Ocean Circulation Experiment data centers listed in the acknowledgments. They cover the North and tropical Atlantic region from the equator to 50°N and from 10°W to 80°W and the entire time interval 1902–1997 in a nonuniform space-time distribution. From that historical database, *Reynaud et al.* [1998] produced an annual climatology (hereinafter referred to as RLMB climatology) on a 1° latitude-longitude grid. In the present work we seek to characterize the vertical variability of related variables, defined as departures from that climatology.

[8] Our statistical analysis is performed in 29 geographic bins of 10°, shown in Figure 1. The size of the bins springs from a compromise between having enough data to allow statistics to converge and being able to show the large-scale variations of the statistics (i.e., from bin to bin). As we calculate EOFs in the form of ensemble statistics (i.e., space-time statistics), a preliminary data processing is performed on the vertical dimension. A surface layer is first discarded so as to limit the contamination of our subsurface EOFs by surface variability. Indeed, the ocean surface variability is driven by atmospheric variabilities at frequencies too high to be properly sampled by the CTD casts used in this study, which inevitably produces aliasing and loss of convergence. The thickness of the surface layer discarded from the analysis is kept constant over each spatial bin but varies horizontally according to the stratification (Figure 1). It is also felt unnecessary to introduce temporal bins since we aim at characterizing the variability of the waters below the layer that is seasonally influenced by the atmosphere. This point is, for example, corroborated by *Emery et al.* [1984], where Brunt-Väisälä frequency profiles, computed from North Atlantic historical hydrographic data, indicate

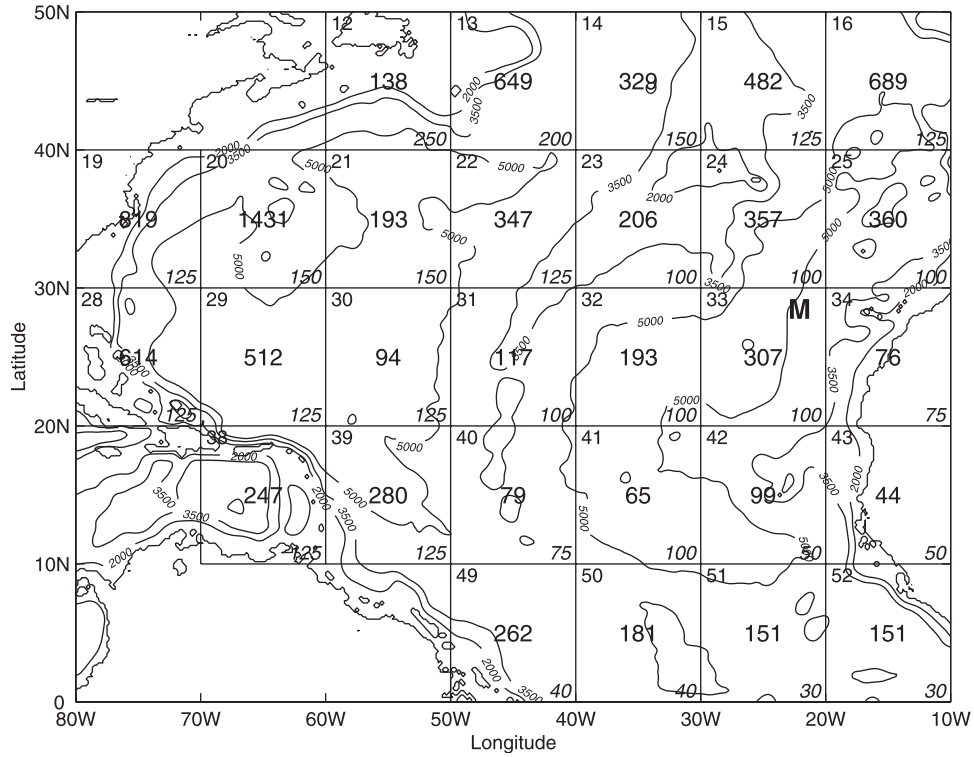

Figure 1. The number of North Atlantic historical hydrographic casts used, shown in the center of the 10° geographic bins. The bin number (upper left) and the thickness (in meters) of the surface layer discarded (lower right) are indicated for each bin. Meddy Sharon (marked with an "M") is shown in bin 33. The bathymetry is outlined, with isobaths at depths 2000, 3500, and 5000 m.

that seasonal variations are largely confined to the upper 250 m. These choices are further discussed in section 3.

[9] Next, a three standard deviation threshold filter is applied to the data set at each level in each bin to eliminate outliers with respect to a Gaussian law. In practice, because the warm and salty Mediterranean lenses (the so-called Meddies) vary in amplitude, not all of them are removed by the filter, even though this phenomenon is likely to be not normally distributed. However, we chose a meddy dated from June 1985 to keep in our analysis, located to the south of the Azores region (bin 33), Meddy Sharon, in order to study its impact on isopycnal statistics. The reader is referred to *Armi et al.* [1989] for a complete description of its path.

[10] The last preprocessing procedure consists of selecting only those profiles reaching at least 2000 m. This enables us to establish a homogeneity of the vertical distribution of data necessary for computing correlations between the different levels. Only 10% of the data pass this step.

[11] Extensive tests show that the procedures described above produce the best convergence of the most significant EOFs. The resulting data set contains 9472 profiles (Figure 1).

3. Methodology

[12] In each bin the basic methodology to calculate the EOFs is similar to that of GDM97, with extensions taking into consideration the basin-wide character of our calculations: large-scale variations of isopycnals in the ocean and statistical separation between surface and deep phenomena.

[13] Like GDM97, we define the ocean bivariate state vector $\mathbf{x}$ in isopycnal coordinates in the following manner:

$$\mathbf{x} = [\theta_1, \ldots, \theta_K, \eta_1, \ldots, \eta_K]^T, \tag{1}$$

where K is the number of vertical levels, θ_k is the compensated potential temperature on the kth isopycnal surface (defined by its potential density anomaly σ_k), and η_k is the vertical displacement of that surface from a given reference level. The potential temperature is here qualified as "compensated" because on a given isopycnal a change in potential temperature induces a direct change in salinity and vice versa. The variables θ_k and σ_k are arbitrarily referenced at 1000 m. As in the case of our observations, equation (1) ranges from the surface layer to 2000 m. The variables θ_k and η_k are defined as departures from the RLMB climatology. By convention, a positive η corresponds to an upward isopycnal displacement.

[14] Our state vector $\mathbf{x}$ is here naturally bivariate in (θ, η) because our data are hydrographic (T, S) profiles. Other choices for $\mathbf{x}$ are possible. For instance, in section 5.3, we calculate univariate η EOFs. However, efficient relationships amongst the variables (θ, η) are also suspected to carry mutual correlations depending on the physical processes studied (e.g., a thermal front associated to a density gradient). The main point in equation (1) is to allow coherent thermal (θ) and dynamical (η) effects to be examined together.

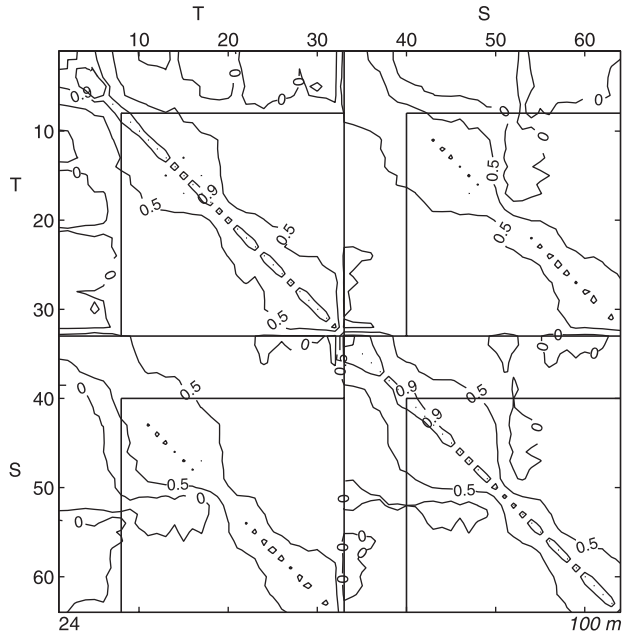

Figure 2. Example of the Azores-Madeira $T(z)$, $S(z)$ correlation matrix from 0 to 2000 m (32 levels). Contours of correlation coefficients are indicated at 0, 0.5, 0.9, and 1. Straight lines delimit the upper ocean from the deep ocean. The number in the lower right refers to the thickness (in meters) of the surface layer discarded as a result of a visual choice.

[15] We work with samples ($\mathbf{x}_i$, $i = 1, N$) of equation (1) obtained from our data set. The isopycnal representation given by equation (1) is determined with the help of the isopycnal transformation, which is univocal wherever vertical stratification is sufficiently marked (see Appendix A). Let us consider a diagonal scaling matrix Σ [see, e.g., *De Mey and Benkiran*, 2002] containing standard deviations of the data set from climatology. We estimate the covariance (COV) matrix of the scaled state vector $\mathbf{x}' = \Sigma^{-1}\mathbf{x}$ empirically as COV $(\mathbf{x}') = \frac{1}{N}\sum_{i=1}^{N} \mathbf{x}'_i \mathbf{x}'^T_i$. Following GDM97, we will calculate the bivariate isopycnal EOFs as the eigenmodes of COV($\mathbf{x}'$).

[16] The problem of the normalization is a major issue in the multivariate EOF calculations. Let us say that there are several methods that depend on physical choices. In our case, there are two reasons to normalize our variables by standard deviations of the data from climatology. First, this method of normalization makes variables dimensionless. It is but one of several different methods a researcher may invent; however, from a statistical aspect it is the most useful and widely accepted method [*Preisendorfer*, 1988]. Second, dimensional EOFs will be related to the variability of the isopycnal displacements and the potential temperature changes on isopycnals observed by in situ data. This suits our needs since we expect isopycnal EOFs to have a large geographical domain of validity.

[17] The choice of a horizontally varying isopycnal grid σ_k ($k = 1, K$) is necessary in our case because the range of isopycnals varies geographically. In each bin an initial 23-level regularly spaced grid has been defined, ranging from the average of the smallest σ values to the average of the largest σ values found in the data in the bin. The last two σ values are discarded to avoid a loss of significance of isopycnal modes at depth caused by weak stratification. This procedure further reduces the depth working range of profiles to ∼1500 m. Each isopycnal grid has in total, K = 21 σ levels. Typically, the σ grid ranges from about σ_1 = 27.5–32.1 kg/m^3 in the equatorial region to σ_1 = 31.2–32.3 kg/m^3 in the high latitudes.

[18] Let us notice that the reference level of our variables is chosen at middepth (1000 m). We tested the use of the so-called "neutral" surfaces in which isopycnal surfaces are referenced to continuously varying pressures in the water column [see *McDougall*, 1987]. In our tests, neutral surfaces gave similar results to isopycnal surfaces in our 10° bins. It is an expected result since in areas our size differences between neutral surfaces and isopycnal surfaces are small.

[19] We also investigate the statistical separation between the surface and subsurface variability. The choice of the thickness of the surface layer discarded from the analysis needs to be justified. The hydrological characteristics of a water column as well as Ekman layer dynamics indicate that the properties of the surface waters, influenced by the surface atmospheric variability, are largely statistically decorrelated from those of the subsurface waters. In a given bin the thickness of the surface layer to be removed from the statistical analysis can thus be determined by considering the $T(z)$, $S(z)$ correlation matrix from 0 to 2000 m. The T, S correlations use z levels, not σ levels, because isopycnal coordinates are not appropriate coordinates close to the surface due to outcropping of isopycnals for instance. The example of the Azores-Madeira region is illustrated in Figure 2. There are four submatrices corresponding to the T, S autocorrelations and cross correlations. At depth, only the correlations between close vertical levels are significant. At the surface, in situ temperature and salinity are highly autocorrelated across layers, which is indicative of the presence of a mixed layer most of the time in the data. The extra diagonal blocks of any submatrix represent the correlations between the surface water and the deep ocean. We use the zero contours of the temperature correlation coefficients to delimit the upper ocean from the deep ocean. In this manner we can visually define the thickness of the surface layer discarded. The criterion is not as clear for the salinity, although there does seem to exist a decorrelation between surface and deep salinity variabilities. The choice of GDM97 (100 m) seems to be in agreement with our criterion in that bin. This method is applied in every bin and works well in accordance with the stratification. As shown in Figure 1, the thickness of the surface layer discarded increases northward and westward from 30 to 250 m. It varies horizontally according to the stratification. Our surface-layer depth is broadly consistent with the map of the annual cycle of mixed-layer depth by *Lamb* [1984, Figure 9] derived from an analysis of in situ temperature profiles, in which the author applied a temperature difference criteria of 1°C. The increase of the depth patterns roughly reflects the heat loss that is experienced by water in regions where temperature and salinity are vertically homogenized through turbulent transports (wind induced or convectively generated), e.g., along the Gulf Stream.

[20] A last methodological comment concerns the calculation of vertical EOFs from real profiles. In well-condi-

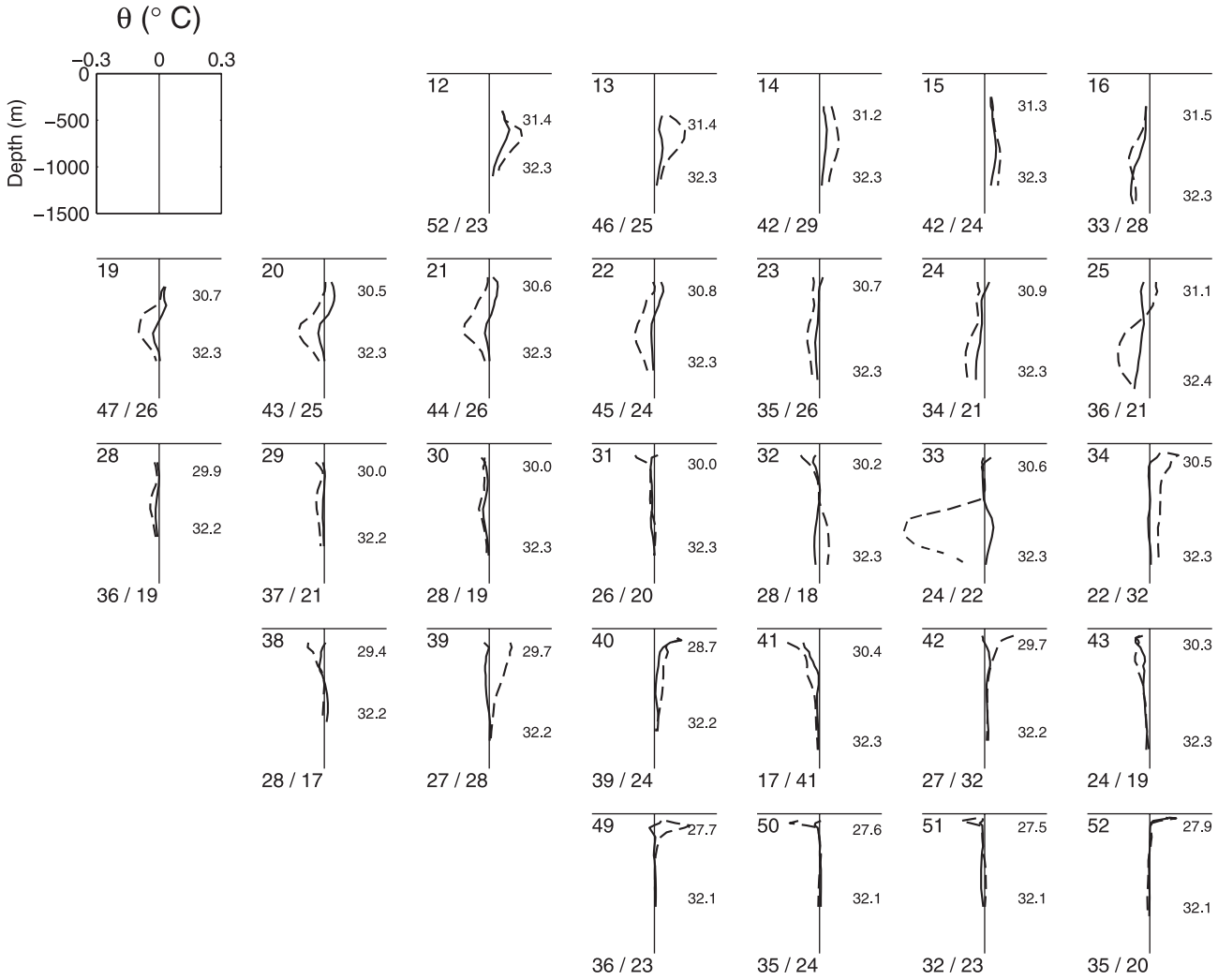

Figure 3. The first two bivariate isopycnal EOFs defined as departures from RLMB climatology: potential temperature (°C) and isopycnal displacement (in meters) as a function of depth (in meters). The percentage of variance explained (PVE) estimates (lower left) given by PVE (λ) = $100 \times \lambda / \Sigma_{m=1}^{2K} \lambda_m$ and the first (upper right) and last (lower right) σ levels (kg/m^3) of the isopycnal grid are indicated for each bin. The first mode is shown as a solid line, and the second one is dashed. In bins 34, 39, 41, and 42 we have intentionally reversed modes 1 and 2.

tioned cases the covariance matrix is symmetric, positive definite, and of full rank. Its eigenvalues are strictly positive and its eigenmodes are orthogonal to each other. In practice, some realizations of **x** are incomplete. The products between two σ levels can be calculated only when data are simultaneously defined at these levels, while the standard deviation from climatology is calculated over all available data at each σ level. Therefore, in practice, the covariance matrix may not be positive definite. However, the method robustly converges for the dominant modes as long as the data sampling is adequate, which was the case in all bins.

4. Isopycnal EOFs in the North and Tropical Atlantic

[21] A major issue when interpreting EOFs is the physical significance of the leading EOF modes. It is not always possible to statistically separate physical processes in the water column. The purpose of this section is to describe the isopycnal EOFs found in the North and Tropical Atlantic and to suggest possible physical interpretations of these modes as far as the isopycnal formulation is concerned.

[22] The two dominant isopycnal EOFs for each bin are presented in Figure 3 for the North and Tropical Atlantic. Modes are ordered following the fractions of variance explained; that is, mode 1 explains more variance than mode 2, and so on. Bivariate modes are showed in dimensional form; that is, they are dimensionalized by the scaling matrix Σ. For an easier interpretation we show the modes on the depth levels of a particular climatological profile of the bin. In bins 34, 39, 41, and 42 we have intentionally reversed modes 1 and 2 because the mode 2 of these bins is similar to the mode 1 of the surrounding ones. In those bins the bivariate mode 2 can directly be compared to the univariate mode 1, shown in section 5.3.

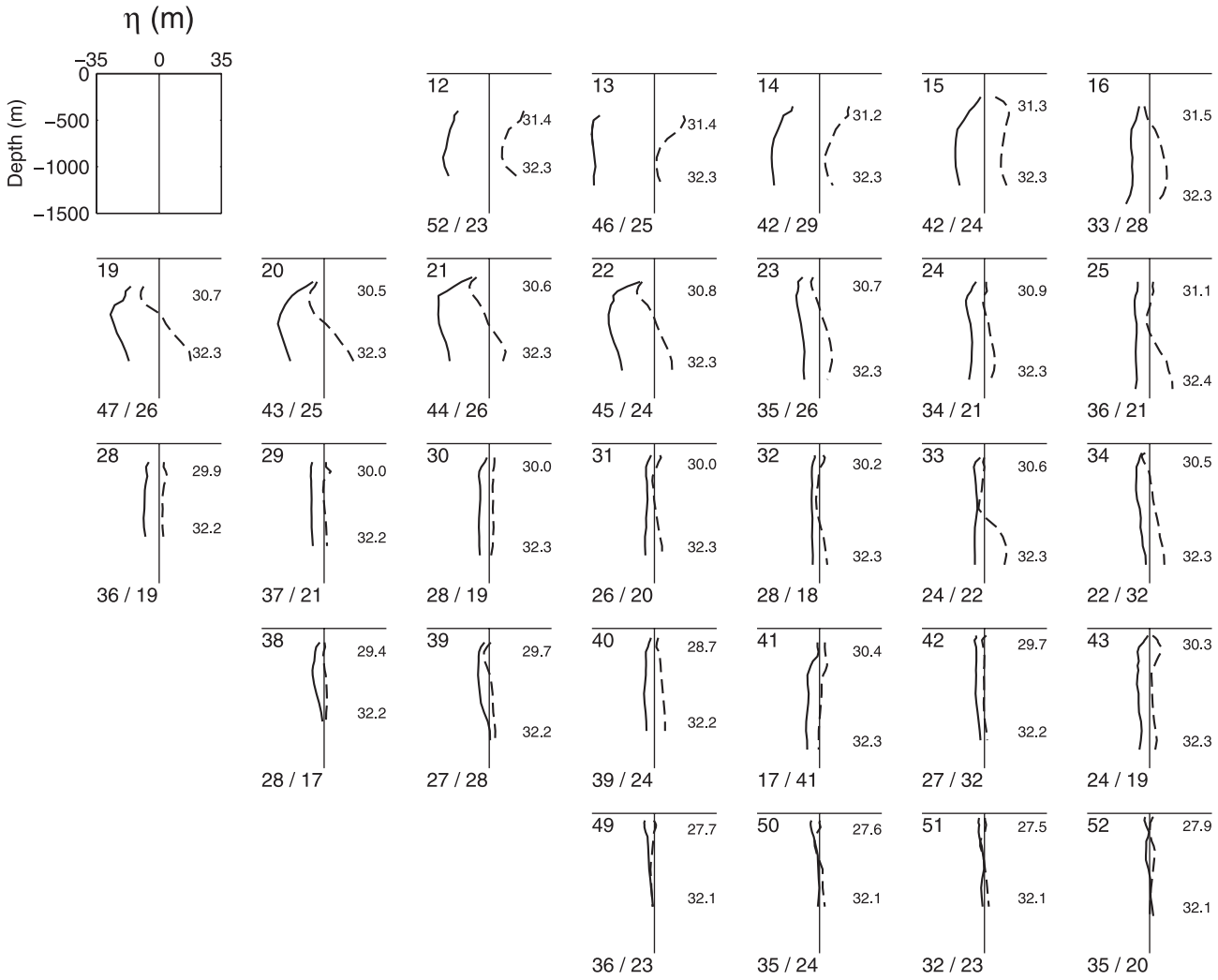

Figure 3. (continued)

[23] The percentage of variance explained (PVE) in normalized form (PVE (λ) = 100 $\times$ $\lambda/\Sigma_{m=1}^{2K}$ λ_m in the bivariate description) by the first two modes ranges from 50 to 70%. The variance explained here is in the (θ, η) space, not in the θ space or η space. Obviously, the PVE estimates presented in this paper depend on the norm that was chosen, i.e., $\langle \mathbf{x}^T \mathbf{x} \rangle$ where $\mathbf{x}$ is bivariate, isopycnic, and centered with respect to RLMB. The angle brackets represent ensemble averaging. PVE estimates cannot be compared when the norm is changed (the total variance is changed), e.g., from bivariate to univariate, as is the case in section 5.3. Therefore the PVE estimates cannot constitute an absolute external criterion in the choice of the state vector.

[24] At first glance in Figure 3 we can see a relative continuity of the shapes of modes from bin to bin. This confirms the large-scale relevance of isopycnal EOFs in the ocean. Ways to take bin discontinuities into account in spatially continuous ocean state estimation problems are discussed in section 6.

[25] In the Azores-Madeira region (bin 24) the EOFs and the associated PVEs are similar to those of GDM97, where data independent from ours were used, the SEMAPHORE cruise data, dated from summer and fall 1993, described by *Eymard et al.* [1996]. Mode 1 (mode 2) accounts for 34% (21%) of the total variance against 38% (25%) of GDM97. GDM97 attributed the first mode to the variability linked to the Azores Front (AF)/Azores Current (AC) and the second mode to the Mediterranean Water (MW). Their analysis seems to be valid in our case as well.

[26] Between 20°N and 30°N and in the eastern half of the 30°–40°N strip (bins 23 to 34), the first empirical mode presents very low variations of temperature on the isopycnal surfaces (except maybe in bins 24 and 25) and a quasihomogeneous vertical displacement of these surfaces. The particular shape of mode 1 accounts for the lifting/lowering of all isopycnals by the same amount without modifying potential temperature on the isopycnals. We name this mode a lifting/lowering mode. Mode 1 is reminiscent of the method put forward by *Cooper and Haines* [1996] (hereinafter referred to as CH96) for the assimilation of altimetry. The water properties and the large-scale potential vorticity on the isopycnals would be conserved by using such a mode to extrapolate the altimeter signal downward, which is the same effect as that of CH96. This link between the purely dynamical considerations of CH96 and our statistical analysis works best in the Sargasso Sea (bin 29), where there is

a full separation along the vertical between the thermal effects and the dynamical effects; that is, $\theta \approx 0$, $\eta \approx 1$ in normalized form.

[27] On the path of the Gulf Stream and its eastward extension up to 40°W (bins 19 to 22), the strong thermocline-intensified baroclinic effects are illustrated by the large amplitude of the η part of the EOF 1, which displays a broad maximum at middepths. As expected, this occurs in a region where the largest values of the first baroclinic Rossby radius of deformation are found [e.g., *Emery et al.*, 1984; *Chelton et al.*, 1998]. We suggest that the large isopycnal displacements visible in the entire water column in mode 1 are consistent with the presence in the data samples of large thermocline displacements in Gulf Stream meanders and rings of either sign. As for mode 2 along the western boundary current, it is represented by the stretching/compression of isopycnals above and below large anomalies of temperature.

[28] In the northwest part of the basin (bins 12, 13, and 19–22) the PVE for mode 1 is high, and simultaneously, the displacements of isopycnals are strong. To give an order of magnitude, mode 1 accounts for ~45% of the total variance, up to 52% in bin 12, while everywhere else this PVE estimate is down to 30–40%. The amplitude of the mode in η is related to the variance of the data set through the dimensionalization of the EOF by the scaling matrix Σ. As the variance of the isopycnal EOFs is directly connected to the space-time variations of perturbation potential energy by means of the isopycnal displacement, we confirm from these statistical considerations that the largest values of potential energy are confined in the western part of the subtropical gyre and are mostly due to thermocline displacement. These considerations are in agreement with the well-known map of eddy potential energy by *Dantzler* [1977, Figure 3] arising from mean-squared isotherm displacements in the thermocline.

[29] Furthermore, we observe that the amplitude in η of the first mode decreases eastward, especially in the zonal band of 30°–40°N. This east-west difference may be due to the presence of the Mid-Atlantic Ridge (MAR), between bins 22 and 23, which would be accompanied by a drop of perturbation potential energy [see *Dantzler*, 1977] and to the fact that the ocean is less stratified in the eastern North Atlantic. A southward decrease of the η part of EOF 1 is visible as well in the 30°–40°W band. As expected, the vertical excursion of isopycnals is smaller at low latitudes due to their packing up near the surface.

[30] Farthest to the northwest (bins 12 and 13), mode 1 exhibits large anomalies of θ with a sign opposite to that of η. It seems to be associated to the lateral excursions of the thermal front (change of θ/S characteristics along isopycnal surfaces) and the density front (change of depth of isopycnals) just southeast of the Grand Banks of Newfoundland, where the Labrador Current (LC), carrying cold and low-salinity waters, clashes with the North Atlantic Current (NAC), carrying warm and salty waters of tropical origin. In support of this interpretation, Figure 4 shows the lateral displacements of such a front, explaining how the variables (θ, η) are of opposite sign on a given isopycnal σ.

[31] Another interesting feature is the northward and westward spreading of the MW from the Gibraltar Strait that influences the shape of mode 2 (and also mode 1 to a lesser extent), in particular, in bins 16, 24, and 25 in the northeast part of the basin (between 30°N and 50°N). A pronounced signature in temperature actually occurs near the isopycnal $\sigma_1 = 32$ kg/m^3, i.e., at ~1000 m depth. This is consistent with the circulation scheme of *Sy* [1988, Figure 18], where the MW tongue slides westward at middepths between the two current systems, the NAC and the AC, at northern (≈48°N) and southern (≈32°N) boundaries, respectively.

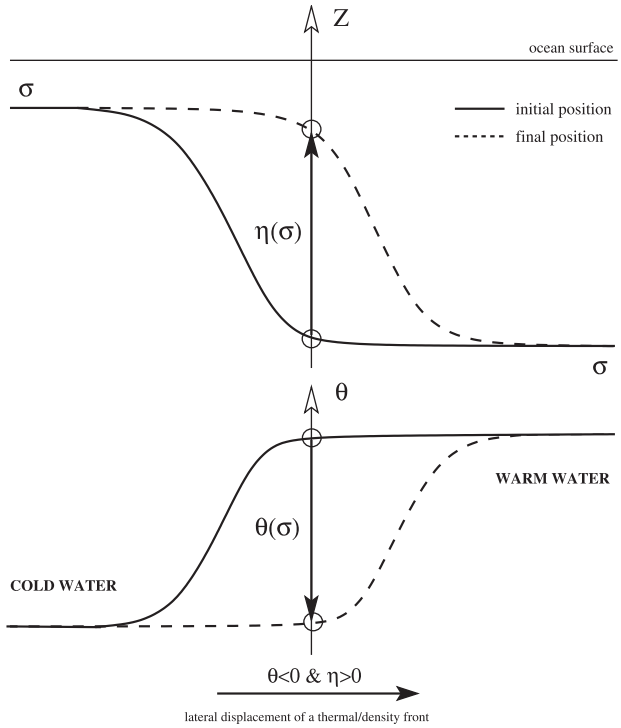

Figure 4. Schematic of the lateral displacements of a thermal/density front (e.g., the Labrador Current/North Atlantic Current front) in an Eulerian coordinate frame. The anomaly of potential temperature θ on the isopycnal σ and the vertical displacement η of that isopycnal are indicated at a given geographical location. These anomalies θ and η are defined as departures from the RLMB climatology. By convention, a positive η corresponds to an upward isopycnal displacement caused by a lateral excursion of the front toward warmer water ($\theta < 0$ and $\eta > 0$). In this schematic the initial position of the front is given by solid lines, the final position by dashed lines. Note that a lateral displacement from warm to cold water introduces anomalies in the opposite sense ($\theta > 0$ and $\eta < 0$).

[32] South of the Azores region (bin 33) the statistical separation of physical processes is well marked in the modes. Mode 1, similar to the lifting/lowering mode of the zonal band 20°–30°N, is slightly influenced at depth by the MW variability, and mode 2 is locally associated to the variability of Meddy Sharon. The meddy core is characterized at $\sigma_1 = 32$ kg/m^3 by the well-known warm anomaly of temperature just above it by a slight lifting up of isopycnals, and below it by a strong lowering (see also the cross sections of density σ_1 of *Armi et al.* [1989, Figure 4]). Thermal and dynamical effects are therefore coupled in mode 2. In the study by GDM97 the isopycnal analysis consistently proved more efficient in separating phenomena

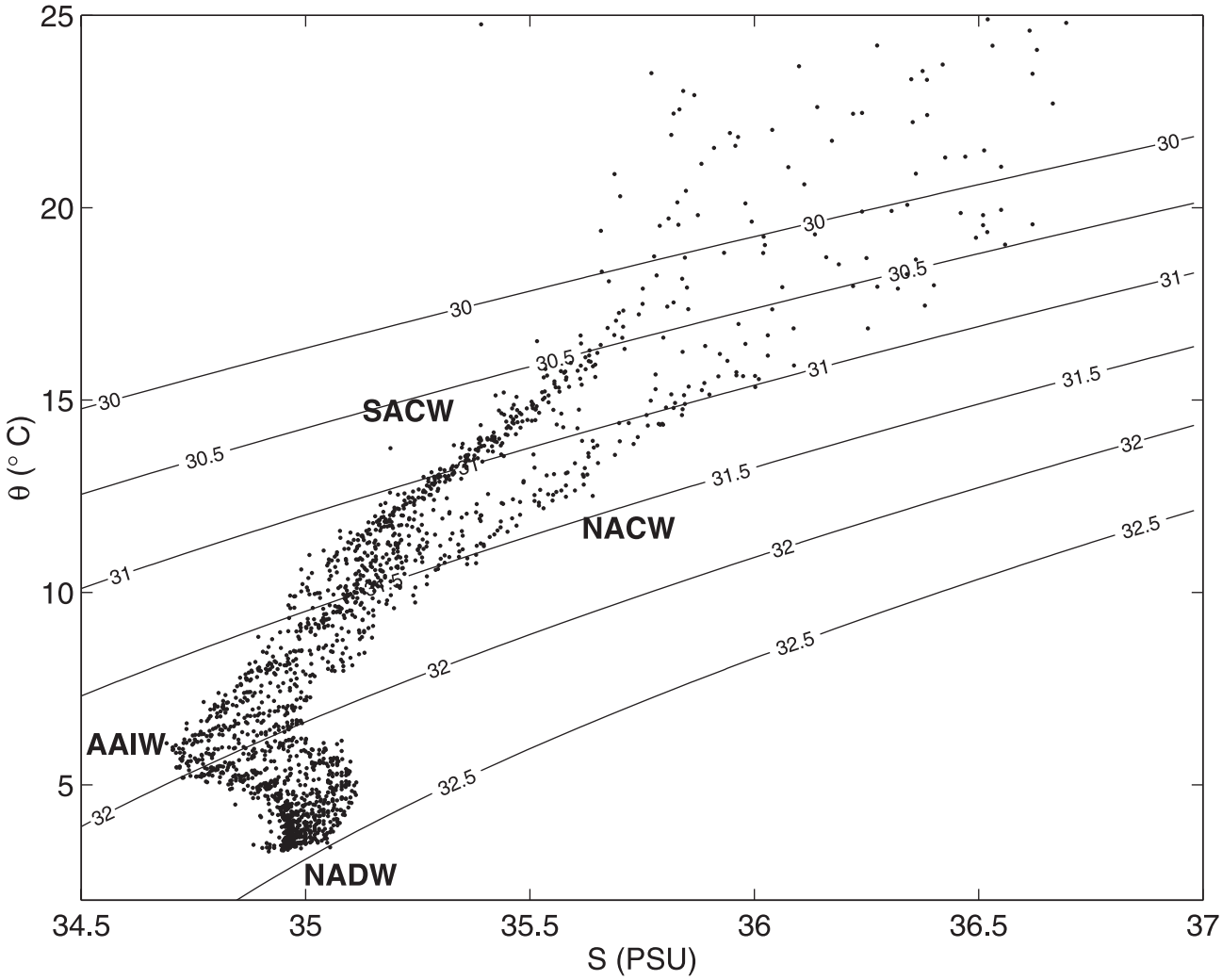

Figure 5. Potential temperature-salinity diagram in bin 42 (10°–20°N, 20°–30°W) from our in situ data set used in the EOF analysis together with acronyms of water masses found in the region. Contours of potential density σ_1 are indicated every 0.5 kg/m^3 from 30 kg/m^3 to 32.5 kg/m^3. The number of data is 1890 (after preprocessing). Data above 50 m depth are discarded in this case. In the range σ_1 = 30–31.5 kg/m^3, data sample the boundary separating the North and South Atlantic central water masses. Abbreviations are AAIW, Antarctic intermediate deep water; NADW, North Atlantic deep water; NACW, North Atlantic central water; SACW, South Atlantic central water; and PSU, practical salinity unit.

in comparison with an analysis in depth coordinates. Nevertheless, the notion of separability of physical processes also depends on the available samples measuring either process simultaneously or not, whatever coordinate system is used. In bin 33 we initially included 88 meddy casts over a total sampling of 307; that is, ∼30% of the casts are meddy casts. Modes 1 and 2 account for approximately the same PVE (24% versus 22%). If we add more meddy casts in the analysis, the variability linked to the meddy will dominate as the most frequent process statistically, which is probably not the case in the natural system.

[33] The isopycnal EOFs of the low latitudes (south of 20°N down to the equator) strongly contrast with those of higher latitudes. Far off the Mauretanean shelf to the west (bins 41 and 42), another case of statistical separation of phenomena is noticeable. Mode 2 is similar to the shape of mode 1 found at midlatitudes and corresponds to the variability of the dynamical structure of the water column (here vertical displacements of isopycnals). The first mode is here clearly surface-intensified in θ from σ_1 = 30 kg/m^3 to σ_1 = 31.5 kg/m^3, while its component in η is almost zero. For reference, in Figure 5, we show the data used in the EOF analysis which sample, in particular, in the same range σ_1 = 30–31.5 kg/m^3, the region located on the boundary separating the North Atlantic central water (NACW) and South Atlantic central water (SACW) masses. *Zenk et al.* [1991] characterized the vertical structure of this frontal zone in the upper 600 m by strong thermohaline vertical gradients and relatively weak density vertical gradients due to a density-compensating effect. This could explain the weak vertical displacement of isopycnals found in mode 1. *Zenk et al.* [1991] also pointed out the general increase in temperature on an isopycnal surface (at 250 m) across the boundary toward the northwest. This could be consistent

with the presence of a warm anomaly of temperature on surface isopycnals visible in mode 1. We thus suggest that mode 1 is associated with the variability of the thermocline discontinuity between the NACW and the SACW. The paths followed by NACW and SACW in the 10°–20°N strip are well depicted in the circulation cartoon of *Schmitz and McCartney* [1993, Figure 9].

[34] In the latitude range 0°–10°N the results are more difficult to interpret. Expectedly, most of the variability explained by modes 1 and 2 is near the surface. The first mode almost exclusively consists of isopycnal displacements, while mode 2 mostly explains near-surface hydrological property changes.

[35] Another striking feature in Figure 3 is the apparent similarity between the shapes of the first two modes in some regions of the North Atlantic (see bins 15, 16, and 40). The isopycnal analysis and/or the data set do not always permit us to fully separate processes occurring in the vertical. We named these modes shuttle modes because they have to be considered together to express the variability linked to the thermohaline and dynamical processes. They may be considered as a failure of the data at hand in some of the bins to permit this type of EOF analysis and to provide clean process separation.

5. Use in State Estimation Problems

5.1. Order Reduction in State Estimation Methods

[36] State estimation consists in calculating the best estimate of the state of a physical system. There are two basic categories of state estimation problems: three-dimensional (3-D) and four-dimensional problems. In the latter category one seeks the best estimate of the evolution of 3-D fields over a given period. In both categories the basic ingredients are data. Other ingredients can include a guess (or background field), usually obtained from a numerical model, or the dynamical model equations themselves (for strong-constraint 4-D methods). Approaches combining model outputs and observations are usually called data assimilation methods. However, it is still possible to obtain an estimate without a model, e.g., by using a climatological guess.

[37] Optimal state estimation uses error estimates of the guess and data to define what optimality means. Generally, one assumes the error statistics to be Gaussian. If this is true, then the best linear unbiased estimator is the best estimator, and one only needs to know the first- and second-order statistical moments of the errors (i.e., biases and covariances). Needless to say, this is still too much to ask in most cases, especially in the case of model errors. In addition, methods to estimate multiparametric errors do exist, but they are very expensive. Therefore the idea of a priori reducing the order of state estimation problems by using precalculated physically consistent structure functions to simplify the error space makes sense. Multivariate EOFs such as those calculated in the previous section are possible candidates if one assumes that the errors can be expressed efficiently on such functions. The reduced-state space (where estimation occurs) can, for instance, be generated by the dominant EOFs. The complementary space, which is left untouched by the reduced-order estimation process, is generally called "null space." EOF-based order reduction in data assimilation problems has, for instance, been studied by *De Mey and Robinson* [1987], *Rienecker and Adamec* [1995], *De Mey* [1997], and *Pham et al.* [1998].

[38] *De Mey and Benkiran* [2002] cover this topic in detail and give the formalism to pose the estimation problem in reduced-order form by using 3-D and vertical EOFs. They also give the conditions for these EOFs to be efficient in simplifying the error space of the problem. We refer the reader to *De Mey and Benkiran* [2002]. In brief, they state that the reduced-space processes must be observable and that the errors in the reduced space and null space must be weakly correlated to each other through the dynamics. The latter condition can, for instance, be achieved if the dominant physical processes in both subspaces are weakly coupled over the timescale considered (EOFs can guarantee this). In section 5.2 we will examine the observability properties of isopycnal EOFs in the perspective of their use to estimate the state of the ocean. As a surface observation, the case of satellite altimetry will be examined with particular attention since the definition of error statistics, e.g., from EOFs, is expected to have a strong influence on the way subsurface variables are inferred. The observability properties for other observing systems could be considered as well; they are not dealt with here.

5.2. Observability From Altimetry

[39] Satellite altimetry is now the primary source of observations for ocean data assimilation. The available satellite altimetry products are generally sea-level anomalies (SLA) from an unknown mean sea surface. They are generally used in models in the form of surface pressure anomalies including barotropic and steric effects. Our purpose in this section is to examine from our in situ data set how SLA and the dominant isopycnal EOFs are connected in the 10° bins defined in section 2. Since in situ data cannot give access to the full contents of SLA, a proxy will be used in the form of dynamic height anomaly (DHA). At any location where data is available, DHA can be expressed as

$$\zeta = -\frac{1}{\rho_0}\int_{\sigma_{\min}}^{\sigma_{\max}} \eta(\sigma)\, d\sigma, \tag{2}$$

where ρ_0 is a mean density, η represents an isopycnal displacement (obtained using the isopycnal transformation in Appendix A), and $(\sigma_{\min}, \sigma_{\max})$ denotes the range of isopycnal surfaces at that location. Equation (2) is in the form of a linear observation equation $\zeta = \mathbf{H}\,\mathrm{x}$, where $\mathbf{H}$ is the isopycnal observation operator for DHA and x is the isopycnal state vector as in equation (1). We should keep in mind that at least a part of barotropic effects, surface steric effects, and some ageostrophic effects are missing from our proxy equation (2) when analyzing the results in this section. This can be formalized by an additional noise term in equation (2) if needed in the formulation of an estimation problem.

[40] The state $\mathbf{x}$ can be expanded over all vertical EOFs (hereinafter referred to as $\mathbf{e}_m$ for mode m) as calculated in section 4:

$$\mathbf{x} = \sum_{m=1}^{2K} x'_m\, \mathbf{e_m}, \tag{3}$$

where x'_m is the projection of $\mathbf{x}$ onto the mth EOF. The contribution of each mode m to the DHA can be examined

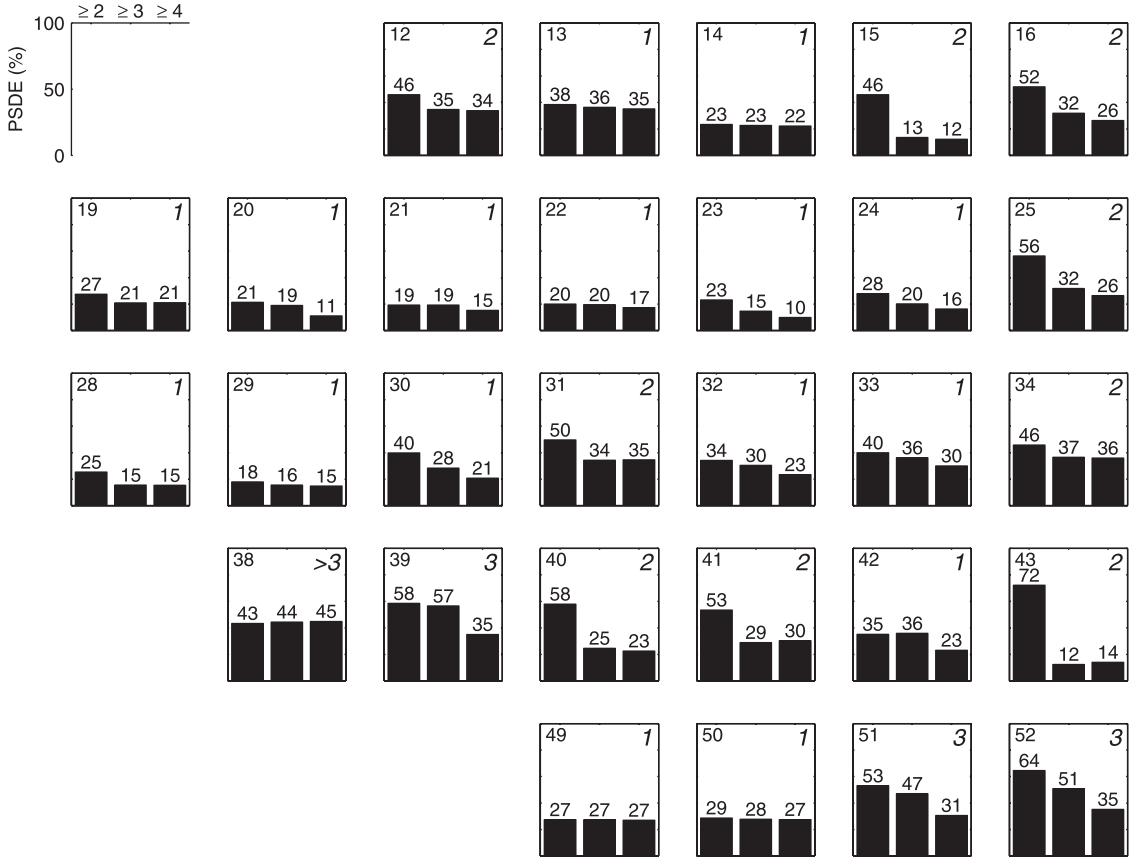

Figure 6. Histogram of percentages of standard deviation (PSDE) by the contribution of modes greater than or equal to 2 ($1000 \times \langle \mu_1^2 \rangle^{1/2} / \langle \zeta^2 \rangle^{1/2}$), 3 ($100 \times \langle \mu_2^2 \rangle^{1/2} / \langle \zeta^2 \rangle^{1/2}$), and ($100 \times \langle \mu_3^2 \rangle^{1/2} / \langle \zeta^2 \rangle^{1/2}$) to the total dynamic height anomaly (DHA) variability. Numbers in upper right of bins indicate the number of dominant modes to be considered in equation (5) to reduce the PSDE estimate to <40%.

by using that expansion in our (linear) DHA observation equation:

$$\zeta = \sum_{m=1}^{2K} \zeta'_m = \sum_{m=1}^{2K} H'_m x'_m, \tag{4}$$

where $H'_m = \mathbf{H}e_m$ is the observation operator restricted to the subspace defined by mode m. It is a scalar at every location. In the purpose of examining the residuals with respect to a truncation of equation (4) to the dominant modes, we also define

$$\mu_M = \zeta - \sum_{m=1}^{M} \zeta'_m, \tag{5}$$

ordering the modes by their decreasing PVE.

[41] DHA was calculated for the casts of the previous section, and its expansion on EOFs (equation 4) was formed. Figure 6 presents histograms with percentages of standard deviation explained (PSDE), $\mathrm{PSDE}(M) = 100 \times \langle \mu_M^2 \rangle^{1/2} / \langle \zeta^2 \rangle^{1/2}$ by the contribution of modes greater than or equal to 2, 3, and 4 (i.e., μ_1, μ_2, and μ_3) to the total surface variability for the North and tropical Atlantic. The smaller these percentages are, the more negligible the contribution of higher modes is to the DHA variability. The histogram allows us to assess the relative contribution of an additional mode in equation (4) and thus to investigate the optimum order of the truncation. We indicate in Figure 6 the number of dominant modes needed to reduce the DHA residual of higher modes to <40% of the total height (this is the value of M for which PSDE(M) is <40%). This 40% threshold may seem large, but it is worth noting that a 40% threshold in standard deviation form only corresponds to a 16% threshold in variance form. The choice of the 40% threshold is indicative and only helpful here for describing results.

[42] The PSDE estimate often decreases or remains constant in a given bin, and its value for $M = 3$ ranges from 10 to 45% with an average value of 24% (it corresponds to a ratio of 1.2 cm over a total of 5 cm). Thus only a few isopycnal modes contribute in a dominant way to the DHA variability in the North Atlantic. In most bins (primarily north of 20°N), one mode (at most two) seems to be enough for reducing the PSDE estimate to <40%. These one-mode boxes are characterized by a weak PSDE for $M = 1$ and a low change of this percentage for M =1, 2, and 3. Especially, note bins 23, 24, 28, and 30, where the addition of mode 2 in equation (5) significantly reduces the PSDE (e.g., from 25 to 15% in bin 28). The two-mode boxes are recognizable by a strong fall of the PSDE from $M = 1$ to $M = 2$. The contribution of the third mode (and the higher modes as well) may not be as negligible in the particular bins 38, 39, 51, and 52 south of 20°N.

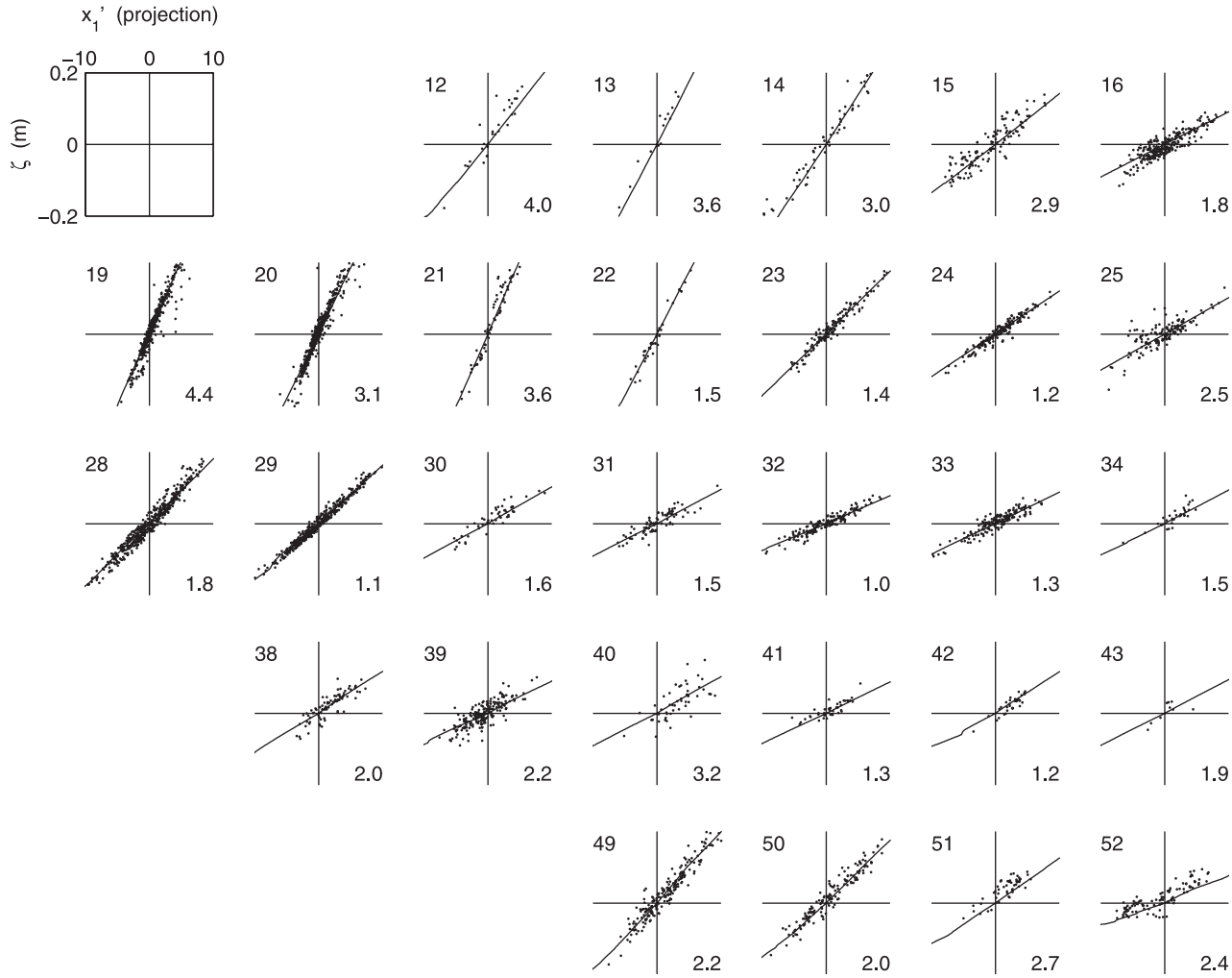

Figure 7. Observability diagrams. Projection of individual casts onto the first two bivariate isopycnal EOFs in x'_1, ζ) space for mode 1 and (x'_2, $\zeta - \zeta'_1$) space for mode 2. The DHA units are in meters. Observability curves are superimposed on scatterplots. Numbers in lower right of bins indicate the rms dispersion: $\langle \mu_1^2 \rangle^{1/2}$ for mode 1 and $\langle \mu_2^2 \rangle^{1/2}$ for mode 2, in centimeters.

[43] We now examine in more detail the reduced-order observability of DHA again using our cast data. In that purpose, only the first two modes were considered. In the case of a one-mode box, mode 1 is necessarily observable from the surface, but we cannot further conclude on the observability of mode 2. For a two-mode box the first two modes are necessarily observable. Figure 7 presents the so-called ''observability diagrams,'' which represent the projection x'_m versus the dynamic height anomaly for the first and second isopycnal modes in the North and tropical Atlantic. The projections of individual casts onto the first two modes are carried out in the (x'_1, ζ) space for mode 1 and (x'_2, $\zeta - \zeta'_1$) space for mode 2 in order to study the structure of modes in terms of observability. The complete profiles from the casts in z are here projected onto the isopycnal grid to form the sampling of complete profiles in σ, provided that the missing values are replaced by those of the closest climatological isopycnal profile.

[44] We call the ''observability curve'' for mode m (m = 1,2) the locus of (y', x'), where $y' = H'_{c,m}x'$, x' ranges from -10 to 10 and $H'_{c,m}$ is the climatological observation operator projected onto mode m, here calculated from a particular climatological profile of the bin. Such a curve permits us to visualize the representation of H'_1 in (x'_1, ζ) space (H'_2 in (x'_2, $\zeta - \zeta'_1$) space), provided that mode 1 (mode 2) is observable in average from altimetry. If not, the observability curve merges with the horizontal axis. On these diagrams the scatter of casts around its observability curve informs us about the ability of the mode to represent by itself the total variability visible from the surface. The rms dispersion for mode 1 (mode 2) in terms of dynamic height $\langle \mu_1^2 \rangle^{1/2}$ ($\langle \mu_2^2 \rangle^{1/2}$), representing the contributions of modes >2 (3), is the result of a repetitive calculation of H'_1 (H'_2) as it depends on the location. It is not exactly the rms distance to the observability curve. On the observability diagrams of Figure 7, we first check that the scatter plots are evenly distributed along the observability curves. That piece of information could not be deduced from the histograms of Figure 6.

[45] In the Azores-Madeira region (bin 24) the DHA observability results are similar to those of GDM97, even

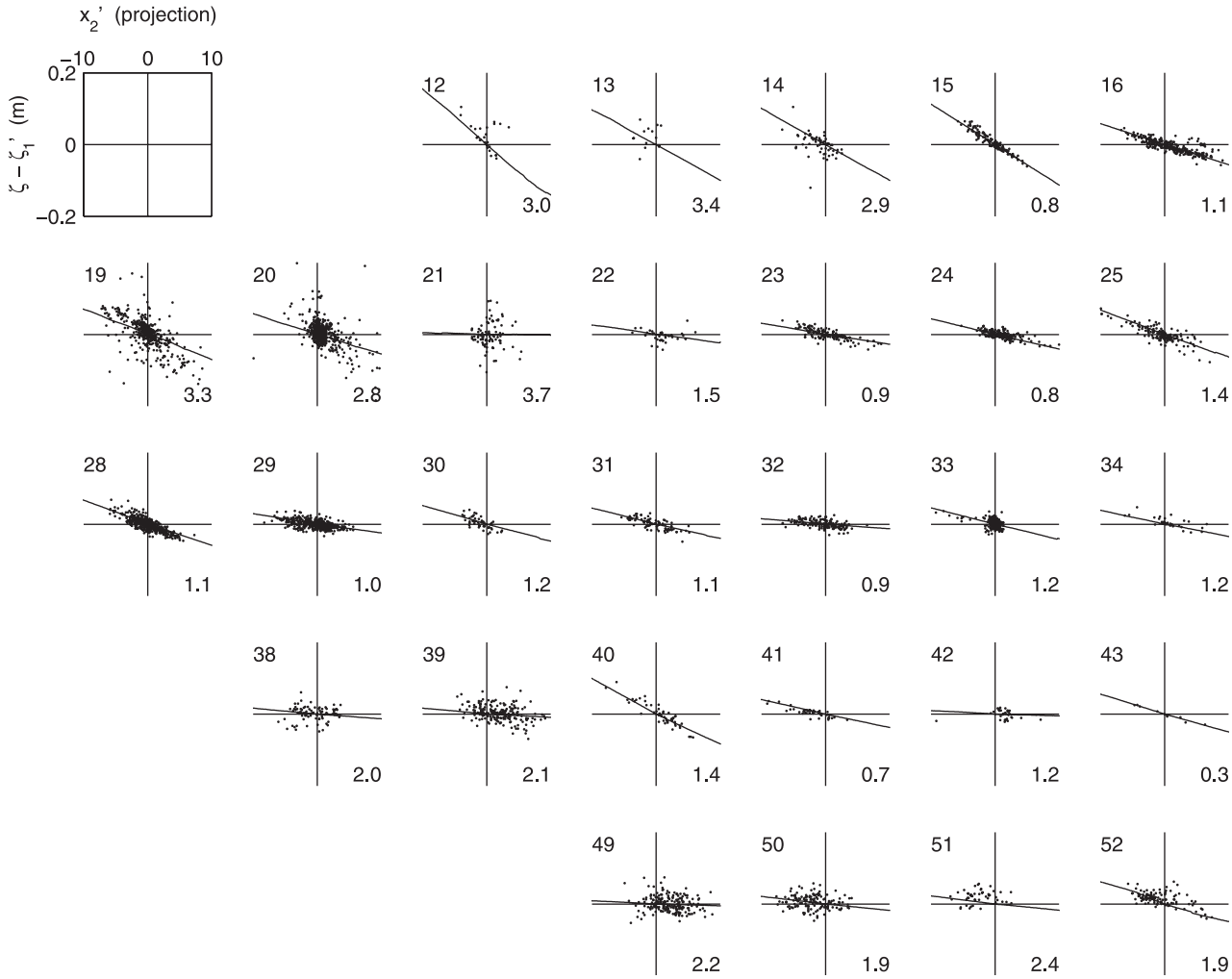

Figure 7. (continued)

in terms of magnitudes of x'_m ($m = 1, 2$) and ζ ($|x'_m| < 10$ and $|\zeta| < 20$ *cm*). For the first mode the scatter due to the contribution of the higher modes is 1.2 cm rms against 1.9 cm, as found by GDM97.

[46] At first glance in Figure 7 the slope of the observability curves for mode 1 is, as expected, nonzero. The scatter around that observability curve appears fairly small in many bins of the North Atlantic with a rms dispersion of only a few centimeters, from 1 (bin 32) to 4.4 cm rms (bin 19). This means that the first isopycnal EOF representing the vertical variability of the dominant dynamical processes in the water column contains most of the DHA variability. When considering one-mode boxes primarily north of 20°N (see Figure 6), there are two cases concerning the observability of mode 2. On one hand, in most one-mode boxes the scatter plot for mode 2 is fairly large or merges together with the horizontal axis. That mode can be considered to be weakly observable in average from the surface. On the other hand, we notice in bins 23, 24, 28, and 30 that the scatter for mode 2 is weak with a nonzero slope of its observability curve. That is, mode 2 is shown as observable from the surface, while its contribution to equation (4) in terms of dynamic height is fairly small. Therefore, as found by *Gavart et al.* [1999], the vertical order-reduction problem in most of the areas north of 20°N is reduced in average to first order.

[47] However, some areas of the North Atlantic (the so-called two-mode boxes in Figure 6) display comparable surface signatures in dynamic height for the first two isopycnal EOFs. The most significant DHA signatures for mode 2 mainly stem from the shuttle modes in bins 15, 16, and 40, which share together the dominant vertical variability (Figure 3). Therefore, in those areas, ζ can be expressed in average at second order.

[48] We also remark in Figure 7 that the smallest scatters for mode 1 can be associated to the vertical EOFs whose shape is the most similar to that of the lifting/lowering mode (e.g., bin 29). Therefore we suspect that a univariate (η) analysis would give more robust results since the number of state variables is reduced. This issue is investigated in section 5.3.

[49] A last comment concerns the surface observability of some of the particular physical processes described through the isopycnal EOFs in section 4. As illustrated in Figure 7, the isopycnal modes linked to the vertical variability of the LC/NAC thermal front (e.g., bin 12 in (x'_1, ζ) space), the Gulf Stream meanders and rings (e.g., bin 20 in (x'_1, ζ) space), and the MW (e.g., bin 25 in (x'_2, $\zeta - \zeta'_1$) space) are

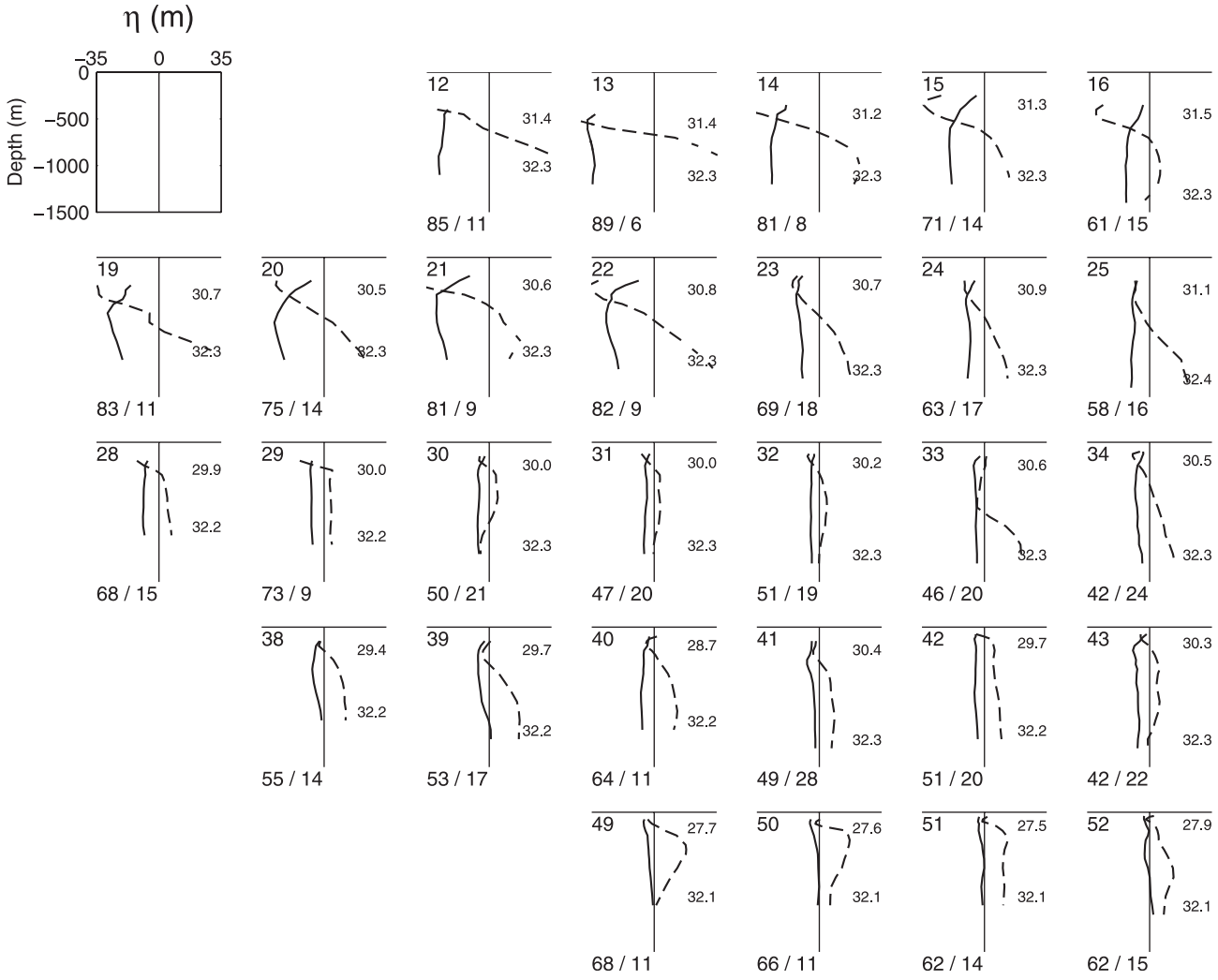

Figure 8. Same as in Figure 2 but with calculation of the first two univariate isopycnal EOFs in η (PVE estimates are given by $\mathrm{PVE}(\lambda) = 100 \times \lambda / \Sigma_{m=1}^{K} \lambda_m$).

represented here by significant surface signatures, which is not so in the case of Meddy Sharon (bin 33 in $(x_2', \zeta - \zeta_1')$ space) and the NACW/SACW frontal zone (e.g., bin 42 in $(x_2', \zeta - \zeta_1')$ space). This does not mean that these latter specific processes are not observable from the surface.

5.3. Restriction to Purely Dynamical Estimation

[50] One could object to the previous analysis that, when assimilating altimetry only, one should not bother with the potential temperature part of the state vector (equation (1)) since the observation equation (2) for DHA is only expressed in isopycnal displacements and ignores compensated potential temperature changes. Also, one could argue that the correlations found between potential temperature and isopycnal displacement in the results of section 4 are only due to sampling and are not real.

[51] We do not negate or confirm those objections in general, although some comments and words of caution have been set forth in section 4. However, it is easy to take into account those a priori assumptions in the EOF analysis and DHA observability analysis and therefore get results which are dynamically more robust. One just has to perform a univariate isopycnal analysis in η, defining the new ocean state vector $\mathbf{x}$ as:

$$\mathbf{x} = [\eta_1, \ldots, \eta_K]^T. \tag{6}$$

[52] Figure 8 presents the first two univariate isopycnal EOFs in η in the North and tropical Atlantic. At first glance the shape and magnitude of the first univariate mode are almost identical to the η part of the first bivariate mode. However, some differences can be seen between Figure 3 and Figure 8. Modes 1 and 2 of bins 34, 39, 41, and 42 are not reversed anymore. The vertical variability shared by the bivariate shuttle modes is now represented by one univariate mode only (e.g., bins 15, 16, and 40). The PVE for that mode ($\mathrm{PVE}(\lambda) = 100 \times \lambda / \Sigma_{m=1}^{K} \lambda_m$ in the univariate description) ranges from 42 to 89%, the greatest values being confined in the northwest region as usual. Its average value in the North Atlantic has largely increased: 64% against only 35% in the bivariate case. These new characteristics suggest that the variability of the dynamical processes is largely condensed in mode 1. The increase of the PVE for mode 1 was of course foreseeable since with one variable η, there are less degrees of freedom to explain. As the variance

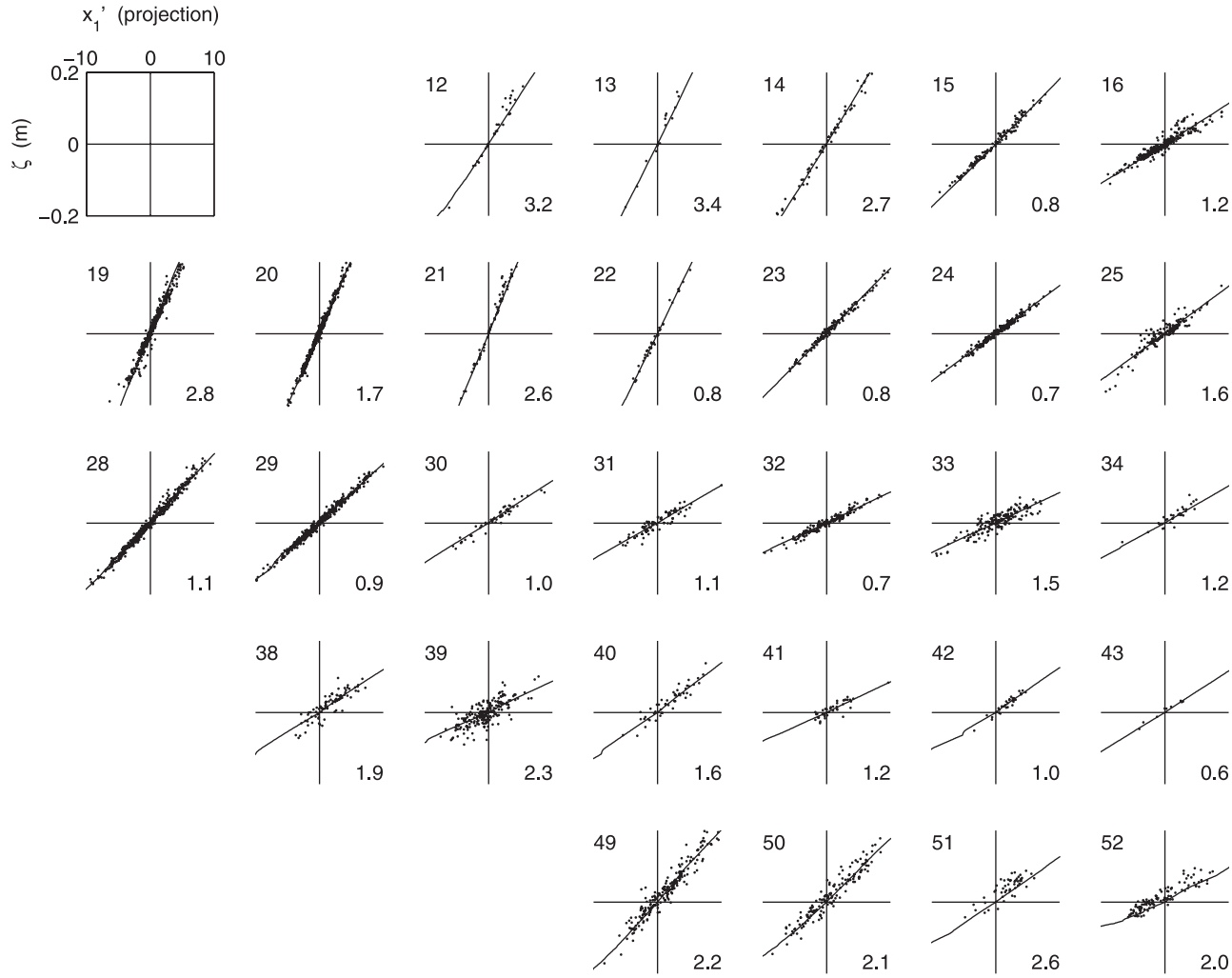

Figure 9. Same as in Figure 7 but with projection of individual casts onto the first univariate isopycnal EOF in η in (x_1', ζ) space.

explained by mode 2 is not significant, we do not attempt to interpret that mode physically.

[53] The univariate DHA observability results for mode 1 in the (x_1', ζ) space are presented in Figure 9 and must be compared to the bivariate projections of Figure 7. At first glance the scatter around the observability curve appears much smaller than before. This time the rms dispersion $\langle \mu_1^2 \rangle^{1/2}$ ranges from 0.6 (bin 43) to 3.4 cm (bin 13) in the North Atlantic. The average improvement of the rms dispersion between the bivariate and univariate calculations is ~27% (1.6 versus 2.2 cm). This confirms that in most cases it is easier to estimate subsurface dynamical variables from altimetry with one univariate mode in η than with one bivariate mode in (θ,η).

6. Summary

[54] The vertical variability of the thermal/dynamical structure of the North and tropical Atlantic ocean defined as the departure from the annual RLMB climatology was investigated from a set of historical hydrographic data. The analysis was performed in terms of vertical empirical orthogonal functions in isopycnal coordinates using a state vector **x** made up of the compensated potential temperature along isopycnals (θ) and isopycnal displacements (η).

[55] This paper focused on studying the coherent thermodynamical and dynamical variability of the regions covered by our data set. The main point of choosing those variables is to allow coherent thermal and dynamical effects to be examined together. Statistical tools such as EOFs are able to quantify such correlations (or lack of) between variables. In particular, GDM97 has illustrated the fact that isopycnal EOFs help to better separate ocean phenomena compared with the z EOFs.

[56] In the first place, the relative continuity of the shape of modes from bin to bin confirmed that the vertical EOFs have a quite extended horizontal domain of validity (of several hundreds of kilometers). We have not calculated explicitly spatial scales of correlation. This may be the subject of a future study.

[57] In the Azores-Madeira region our dominant isopycnal EOFs were very similar to those of GDM97. The robustness of the EOFs calculated from two different data sets (synoptic and historical) was therefore illustrated.

[58] The first two isopycnal EOFs of the North Atlantic ocean, calculated in 29 geographic bins of 10°, accounted

together for ~50–70% of the total variance. The most frequent process statistically described by mode 1, mostly visible north of 20°N, represented a quasihomogeneous vertical displacement of the isopycnal surfaces in the water column with a quasiconservation of potential temperature on those surfaces. That mode was strongly modified by thermocline intensified baroclinic effects along the path of the Gulf Stream up to 40°W. Our isopycnal statistics showed for the midlatitudes the validity of the purely dynamical method put forward by CH96, based originally on a conservation principle of *T*, *S* properties or large-scale potential vorticity on isopycnals, for the assimilation of altimetry. Some physical interpretations of the vertical EOFs were also suggested in several areas as far as the isopycnal formulation was concerned (e.g., some thermal fronts, the Mediterranean outflow, water lenses, or ''meddies''). The present work illustrates the fact that the separability of physical processes depends on the configuration of the observational system measuring either process together or separately. Examples of nonseparability using the isopycnal analysis were given by the shuttle modes, which have to be considered together to express the vertical variability. The correct procedure for separating phenomena systematically would probably involve using the number of degrees of freedom explained by the processes, but we have no simple way of estimating this parameter.

[59] This work confirmed the validity of the ideas of GDM97 over the entire North Atlantic ocean. The potential use of the isopycnal EOFs in state estimation and data assimilation problems was discussed. They are possible candidates to reduce the order of state estimation problems, if one assumes that background and forecast errors can efficiently be expressed on such functions. The estimation occurs in the reduced-state space which is generated by only a few EOFs. The EOFs are to be used to simplify the error subspace in a state estimation problem incorporating all kinds of data (including altimetry) not to extrapolate directly at depth. The depth extrapolation is handled via the observation operator and forecast error covariances. Good observability properties of these EOFs are required to estimate the state of the ocean. These observability properties were studied in the case of satellite altimetry; that is, we examined how the dominant isopycnal EOFs were connected to SLA. As an attempt to discuss the order of the truncation process, percentages of standard deviation explained by the contribution of modes higher than 2, 3, and 4 to the total DHA variability were calculated. In most bins the order of the truncation here arbitrary defined by a 40% threshold of the PSDE was reduced to one mode (primarily north of 20°N) or two modes observable in average from altimetry. It was found that the dominant isopycnal EOF representing the vertical variability of the thermal/dynamical processes was able to account for most of the surface dynamic height variability with a rather normally distributed error of only a few centimeters. That there are limited degrees of variability is not new in itself, but the point here is to show vertical functions derived from empirical data analysis that explain most of the sea-level changes. From that result one can argue that it is worth to extrapolate the altimetric signal at depth using these functions to infer subsurface variables. The tight relationship between sea-level variability and subsurface variability has been studied in the past [see, e.g., *Carnes et al.*, 1990; *Miller and Cheney*, 1990; *Gilson et al.*, 1998] and underlies the importance of satellite altimetry as part of a global observing system.

[60] One may search dynamically more robust results by performing a univariate isopycnal analysis in η, leaving coherent thermal effects out. As a result, the variability became even more monochromatic (one mode) everywhere, and the dominant univariate mode explained more of the DHA signature than the bivariate one. It is not an unexpected result since we have reduced the number of state variables. It seems easier to estimate subsurface dynamical variables from altimetry with one univariate mode in η than with one bivariate mode in (θ, η) according to our proxy (equation (2)). This univariate analysis in η also expands the assimilation technique put forward by CH96 because it allows much more general vertical displacement structures. Therefore univariate η EOFs are probably good candidates for purely dynamical estimation studies.

[61] However, in areas where efficient relationships amongst the variables (θ, η) are suspected to carry mutual correlations (e.g., some thermal fronts such as the one associated with LC and NAC), one should probably use the bivariate isopycnal EOFs, which allow coherent thermal (θ) and dynamical (η) effects to be considered together [e.g., *Gavart et al.*, 1999] in the Azores Front/Azores Current system.

[62] In the low latitudes, potential temperature on isopycnals plays a central role. The first bivariate EOF was indeed found to be surface intensified in θ, while its component in η was almost zero. We calculated univariate isopycnal EOFs in θ (not shown in this paper). They explained ~50% of the total variance. Most of the time, higher order bivariate EOFs intensified in temperature have one-to-one correspondence with the dominant univariate EOFs in θ. A similar analysis also showed at higher latitudes that potential temperature on isopycnals does play a role.

[63] In this paper, EOFs were calculated without taking the surface layer into account. Concerning the practical use of isopycnal EOFs, there is a way to extend the domain of validity of the EOFs to the surface layer and deep ocean. One can assume that vertical displacements of isopycnals are zero at the surface of the ocean and remain constant at depth. Isopycnal EOFs can be extrapolated in that manner. When assimilating, for instance, we use the EOFs to represent the model error, and we make the hypothesis that there is no error in the surface layer. Clearly, one must go beyond that point if there is a clear ambition to change the surface layers with data assimilation. This probably cannot be done with isopycnal EOFs and is the subject of ongoing work. One possible practical approach for the time being is to assume that only the forcings, not data assimilation, control the surface layer.

[64] A last comment concerns the use of discontinuous bin-dependent modes in spatially continuous ocean state estimation problems. One interesting possibility, applied by *De Mey and Benkiran* [2002] in the case of assimilation in a Mediterranean model, consists in expanding the background error variances in the space of EOFs and allows the error variance for each mode to be zero everywhere except in the region in which it is defined (here, a $10 \times 10^{\circ}$ bin). A ramp function can then be used to provide a smooth connection of error variances between regions.

[65] The statistical tool of the isopycnal EOFs is being used in separate studies to set up reduced-order data assimilation schemes incorporating satellite altimetry in the North Atlantic. We believe that this isopycnal approach can be used in other regions of the world ocean with good historical hydrographic data and relevant climatologies.

Appendix A: The Isopycnal Transformation

[66] The isopycnal transformation allows us to determine the isopycnal representation of an individual cast measured on standard levels [e.g., *Gavart*, 1996]. Considering potential temperature T_k' and salinity S_k' on a standard level z_k', potential density σ_k' is given by the equation of state $\mathcal{F}$ [*UNESCO*, 1981]:

$$\sigma_{k'} = \mathcal{F}(T_{k'}, S_{k'}, z_{k'}, \text{ref} = 1000 \text{ m}). \tag{A1}$$

[67] If σ_k defines the isopycnal grid, then T_k and z_k are determined on the isopycnal surface σ_k as a result of a linear interpolation, provided that the ocean is sufficiently stratified:

$$(T_{k'}, z_{k'})_{(\sigma_{k'})} \overset{\text{interpolation}}{\longleftrightarrow} (T_k, z_k)_{(\sigma_k)}. \tag{A2}$$

[68] The isopycnal transformation $\mathcal{I}$ is thus defined by:

$$\mathcal{I} : (T_{k'}, S_{k'})_{(z_{k'})} \longmapsto (T_k, z_k)_{(\sigma_k)}. \tag{A3}$$

[69] As we consider the vertical variability as departure from climatology, the transformation $\mathcal{I}$ gives access to the isopycnal representation:

$$\delta\mathcal{I} : (\delta T_{k'}, \delta S_{k'})_{(z_{k'})} \longmapsto (\theta_k, \eta_k)_{(\sigma_k)} \tag{A4}$$

with

$$\begin{cases} \theta_k &= T_k(\mathrm{s_k}) - T_{k\mathrm{clim}}(\sigma_k) \\ \eta_k &= z_k(\mathrm{s_k}) - z_{k\mathrm{clim}}(\sigma_k). \end{cases} \tag{A5}$$

[70] **Acknowledgments.** We are grateful to Richard Coleman of the University of Tasmania, Hobart, Australia, for his constructive comments on an earlier version of the manuscript. We thank the two anonymous reviewers for their careful review of the paper. The detailed comments were very useful in improving the quality of the paper. We thank Thierry Reynaud from the Clipper project for providing his climatology and for his help in obtaining the historical CTD profiles of the North and tropical Atlantic. The following people are acknowledged for making their data available to us: Young-Hyang Park (CIVA-1 and CIVA-2 cruises, Muséum National d'Histoire Naturelle), Eberhard Fahrbach (Antarctic data, Alfred-Wegener-Institut für Polar- und Meeresforschung), Gregorio Parrilla Barrera (A5 cruise data, Instituto Español de Oceanografia), William M. Smethie, Jr. (A15 cruise data, Lamont-Doherty Earth Observatory), Gerold Siedler (A10 cruise data, Institut fuer Meereskunde an der Universitaet Kiel), Michel Arhan and Herle Mercier (Cither-2, Cither-3 and Romanche, Ifremer), and Yves Gouriou (Etambot-1 and Etambot-2, Ifremer). Support for this work was provided to Pascal Faucher by a DGA/CNRS fellowship, to Michel Gavart by SHOM/CMO, and to Pierre De Mey by CNRS and the European Union ENVIRONMENT programme (contract ENV4-CT98-0744).

References

Armi, L., D. Hebert, N. Oakey, J. F. Price, P. L. Richardson, T. Rossby, and B. Ruddick, Two years in the life of a Mediterranean salt lens, *J. Phys. Oceanogr.*, *19*, 354–370, 1989.

Bleck, R., and L. T. Smith, A wind-driven isopycnic coordinate model of the North and equatorial Atlantic ocean, 2, Model development and supporting experiments, *J. Geophys. Res.*, *95*, 3273–3286, 1990.

Carnes, M. R., J. L. Mitchell, and P. W. deWitt, Synthetic temperature profiles derived from Geosat altimetry: Comparison with air-dropped expendable bathythermograph profiles, *J. Geophys. Res.*, *95*, 17,979–17,992, 1990.

Chassignet, E., Rings in numerical models of ocean general circulation: A statistical study, *J. Geophys. Res.*, *97*, 9479–9492, 1992.

Chelton, D. B., R. A. Deszoeke, M. G. Schlax, K. El Naggar, and N. Siwertz, Geographical variability of the first baroclinic Rossby radius of deformation, *J. Phys. Oceanogr.*, *28*, 433–460, 1998.

Cooper, M., and K. Haines, Altimetric assimilation with water property conservation, *J. Geophys. Res.*, *101*, 1059–1077, 1996.

Dantzler, H. L., Jr., Potential energy maxima in the tropical and subtropical North Atlantic, *J. Phys. Oceanogr.*, *7*, 512–519, 1977.

De Mey, P., Data assimilation at the oceanic meso-scale: A review, *J. Meteorol. Soc. Jpn.*, *75*, 415–427, 1997.

De Mey, P., and M. Benkiran, A multivariate reduced-order optimal interpolation method and its application to the Mediterranean basin-scale circulation, in *Ocean Forecasting: Conceptual Basis and Applications*, edited by N. Pinardi, Springer-Verlag, New York, pp. 281–305, 2002.

De Mey, P., and A. R. Robinson, Assimilation of altimeter eddy fields in a limited-area quasi-geostrophic model, *J. Phys. Oceanogr.*, *17*, 2280–2293, 1987.

Emery, W. J., W. G. Lee, and L. Magaard, Geographic and seasonal distributions of Brunt-Väisälä frequency and Rossby radii in the North Pacific and North Atlantic, *J. Phys. Oceanogr.*, *14*, 294–317, 1984.

Eymard, L., Study of the air-sea interactions at the mesoscale: The SEMAPHORE experiment, *Ann. Geophys.*, *14*, 986–1015, 1996.

Fischer, M., and M. Latif, Assimilation of temperature and sea level observations into a primitive equation model of the tropical Pacific, *J. Mar. Syst.*, *6*, 31–46, 1995.

Fukumori, I., and C. Wunsch, Efficient representation of the North Atlantic hydrographic and chemical distributions, *Prog. Oceanogr.*, *27*, 111–195, 1991.

Gavart, M., Modélisation et assimilation de données dans un modèle de circulation océanique à méso-échelle: Application à la campagne semaphore, doctoral thesis, 248 pp., Université Paul Sabatier, Toulouse, 1996.

Gavart, M., and P. De Mey, Isopycnal EOFs in the Azores Current region: A statistical tool for dynamical analysis and data assimilation, *J. Phys. Oceanogr.*, *27*, 2146–2157, 1997.

Gavart, M., P. De Mey, and G. Caniaux, Assimilation of satellite altimeter data in a primitive equation model of the Azores-Madeira region, *Dyn. Atmos. Oceans*, *29*, 217–254, 1999.

Gilson, J., D. Roemmich, B. Cornuelle, and L. L. Fu, Relationship of TOPEX-POSEIDON altimetric height to steric height and circulation in the North Pacific, *J. Geophys. Res.*, *103*, 27,947–27,965, 1998.

Hayes, S. P., and D. Halpern, Correlation of current and sea level in the eastern equatorial Pacific, *J. Phys. Oceanogr.*, *14*, 811–824, 1984.

Lamb, P. J., On the mixed-layer climatology of the North and tropical Atlantic, *Tellus, Ser. A*, *36*, 292–305, 1984.

Maes, C., A note on the vertical scales of temperature and salinity and their signature in dynamic height in the western Pacific Ocean: Implications for data assimilation, *J. Geophys. Res.*, *104*, 11,037–11,048, 1999.

McDougall, T. J., Neutral surfaces, *J. Phys. Oceanogr.*, *17*, 1950–1964, 1987.

Mellor, G. L., and T. Ezer, A Gulf Stream model and an altimetry assimilation scheme, *J. Geophys. Res.*, *96*, 8779–8795, 1991.

Mercier, H., and A. Colin de Verdière, Space and time scales of mesoscale motions in the eastern North Atlantic, *J. Phys. Oceanogr.*, *15*, 171–183, 1985.

Mercier, H., M. Ollitrault, and P. Y. Le Traon, An inverse model of the North Atlantic general circulation using Lagrangian float data, *J. Phys. Oceanogr.*, *23*, 689–715, 1993.

Miller, L., and R. Cheney, Large-scale meridional transport in the tropical Pacific Ocean during the 1986–1987 El Niño from Geosat, *J. Geophys. Res.*, *95*, 17,905–17,919, 1990.

New, A., and R. Bleck, An isopycnic model study of the North Atlantic, part II, Interdecadal variability of the subtropical gyre, *J. Phys. Oceanogr.*, *25*, 2700–2714, 1995.

Pedlosky, J., *Geophysical Fluid Dynamics*, 2nd ed., 710 pp., Springer-Verlag, New York, 1987.

Pham, D. T., J. Verron, and M. C. Roubaud, A singular evolutive extended Kalman filter for data assimilation in oceanography, *J. Mar. Syst.*, *16*, 323–340, 1998.

Preisendorfer, R. W., *Principal Component Analysis in Meteorology and Oceanography*, 425 pp., Elsevier Sci., New York, 1988.

Reynaud, T., P. Legrand, H. Mercier, and B. Barnier, A new analysis of

hydrographic data in the Atlantic and its application to an inverse modelling study, *Int. World Ocean Circ. Exp. Newsl.*, *32*, 29–31, 1998.

Rienecker, M. M., and D. Adamec, Assimilation of altimeter data into a quasigeostrophic ocean model using optimal interpolation and EOFs, *J. Mar. Syst.*, *6*, 125–143, 1995.

Schmitz, W. J., Jr., and M. S. McCartney, On the North Atlantic circulation, *Rev. Geophys.*, *31*, 29–49, 1993.

Smith, L. T., E. P. Chassignet, and R. Bleck, The impact of lateral boundary conditions and horizontal resolution on North Atlantic water mass transformations and pathways in an isopycnic coordinate ocean model, *J. Phys. Oceanogr.*, *30*, 137–159, 2000.

Sy, A., Investigation of large-scale circulation patterns in the central North Atlantic: The North Atlantic current, the Azores current, and the Mediterranean water plume in the area of the Mid-Atlantic Ridge, *Deep-Sea Res.*, *35*, 383–413, 1988.

UNESCO, Tenth report of the joint panel on oceanographic tables and standards,*UNESCO Tech. Pap. in Mar. Sci.*, *37*, Paris, 1981.

Wunsch, C., The vertical partition of oceanic horizontal kinetic energy, *J. Phys. Oceanogr.*, *27*, 1770–1794, 1997.

Zenk, W., B. Klein, and M. Schröder, Cape Verde Frontal Zone, *Deep-Sea Res.*, *38*, S505–S530, 1991.

P. De Mey and P. Faucher, Laboratories d'Eludes ed Géopposite et Océanographie Spatiales (LEGOS), UMR5566/CNRS/CNES/UPS, 18, Avenue Edouard Belin, Toulouse Cedex 4 F-31401, France. (Pierre.De-Mey@cnes.fr; Pascal.Faucher@cnes.fr)

M. Gavart, Bureau de Recherches et d'Eludes SHOM-Météo, LEGOS, 18 Avenue E. Belin, Toulouse Cedex 4 F-31401, France. (Michel.Gavart@cnes.fr)